Silica/poly(vinylidene fluoride) porous composite membranes for lithiumion battery separators

C.M. Costa [a,b,*,1], M. Kundu [c,d,1], V.F. Cardoso [a,e], A.V. Machado [f], M.M. Silva [b], S. Lanceros-Méndez [g,h,**]

[a] Centro de Física, Universidade do Minho, Campus de Gualtar, 4710-057 Braga, Portugal

[b] Centro de Química, Universidade do Minho, Campus de Gualtar, 4710-057 Braga, Portugal

[c] Department of Chemistry, SRM University, Kattankulathur, 603203 Tamil Nadu, India

[d] Department of Material Science and Engineering, Norwegian University of Science and Technology (NTNU), NO-7491 Trondheim, Norway

[e] CMEMS-UMinho, Universidade do Minho, DEI, Campus de Azurém, 4800-058 Guimarães, Portugal

[f] Institute for Polymers and Composites/i3N, University of Minho, 4800-058 Guimarães, Portugal

* BCMaterials, Basque Center for Materials, Applications and Nanostructures, UPV/EHU Science Park, 48940 Leioa, Spain

[h] IKERBASQUE, Basque Foundation for Science, 48013 Bilbao, Spain

Keywords:
PVDF
Silica
Separators
Lithium-ion batteries

Abstract

Separator membranes based on silica/poly(vinylidene fluoride) composites were prepared by a non-solvent induced phase separation (NIPS) process with different air exposure times before immersion in a water coagulation bath and for the same filler content of 20wt%. Mesoporous silica spheres (SS) of ~ 400 nm average diameter were synthetized by sol-gel method and dispersed into the polymer matrix.

It was demonstrated that the morphology, degree of porosity, uptake value and electrical properties of the composite membranes were influenced by the time of exposure to air and the presence of SS.

The membranes were assembled in $Li/C - LiFePO_4$ half-cells and the best cycling performance was obtained for the composite membrane after 1 min exposure to air. This membrane shows an ionic conductivity of $0.9 mScm^{-1}$. Moreover, at a very high rate of 2 C and after 50 cycles, the discharge capacity value, a capacity retention and a capacity fade are $95 mAhg^{-1}$, 79% and 4%, respectively. Thus, it was concluded that this novel separator membrane is suitable for lithium-ion battery applications.

Introduction

Energy is among the most relevant global problems that modern society must solve in the coming years, where it is necessary to guarantee access to energy for all and reduce the processing and consumption of fossil fuels [1].

Considering the increasing energy demands arising from the continuous technological development and advances in portable electronic products (cell phones, computers) and electric vehicles (EV), and hybrid electric vehicles (HEV), it is necessary to increase the efficiency of storage systems for clean energy providing from renewable energy resources [2].

The most relevant electrochemical energy storage devices are lithium ion batteries, as they are lighter, show higher energy density, lower self-discharge, no memory effect, prolonged service-life, higher number of charge/discharge cycles and environmental friendliness, when compared to related systems [3,4].

Lithium ion batteries are composed of anode, cathode and separator, the separator being placed between the electrodes, which serves as a medium for charge transfer [5].

Typically, the separators are constituted by a porous polymeric matrix of different types, the most used being poly(ethylene) (PE) [6], poly(propylene) (PP) [7], poly(ethylene oxide) (PEO) [8,9], poly(acrylonitrile) (PAN) [8,10], poly(vinylidene fluoride) (PVDF) and its copolymers (PVDF-co-trifluoroethylene, PVDF-TrFE, PVDF-co-hexafluoropropylene, PVDF-HFP and PVDF-co-chlorotrifluoroethylene, PVDF-CTFE) [11-13]. Those polymer matrices are soaked by the electrolyte solution, i.e, a liquid electrolyte where salts are dissolved in solvents, water or organic molecules. In order to improve thermal, mechanical and electrochemical properties of the separator, different

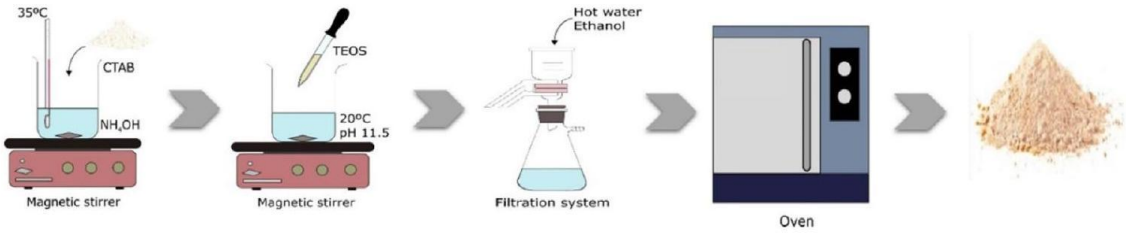

Fig. 1. Main experimental steps for the synthesis of mesoporous SS by the sol-gel method.

fillers may be added to the polymer matrix [14]. Typically, fillers are divided into two classes, active fillers based on lithium salts and passive fillers based on inert ceramic oxides, ferroelectric materials, clays, carbonaceous and molecular sieves being the most relevant [15].

The most commonly used passive fillers are inert ceramic oxides, among which the most important are silica (SiO_2), titanium dioxide (TiO_2) and alumina (Al_2O_3) [14].

Silica (SiO_2) is one of the most investigated inert ceramic fillers as it increases the ionic conductivity of the polymer matrix through a decrease of the crystallinity of the polymer, supporting the free movement of the Lithium ions through the segmental motion of the polymer chains [16].

Considering the suitable mechanical strength of porous polypropylene (PP) separators and for improving its electrochemical performance for lithium ion batteries, coatings were performed with SiO_2/ PVDF-HFP [17] and SiO_2 /PVDF [18,19] composites, leading to improved electrolyte uptake and ionic conductivity, showing also lower interfacial resistance and improving cyclability of cells.

PVDF electrospun separators loaded with different amount of inorganic nanoparticles of SiO_2 were successfully produced and it was found that SiO_2 enhances the rate of electrolyte uptake due to its high polarity and improves the insulating properties of the membranes at high temperatures [20].

Further, hybrid PVDF/polyacrylonitrile (PAN) membranes highly loaded with silica nanoparticles (67.5wt%) show superior discharge capacity and cyclic performance even at temperature higher than 120°C, in comparison with pristine membrane [21]. PVDF/poly(methyl methacrylate), PMMA/SiO_2 composite membrane produced by electrospinning, the introduction of PMMA and SiO_2 decreasing the crystallinity of PVDF, improving the absorption of liquid electrolyte and leading to higher ionic conductivity ($4mScm^{-1}$) and lower interfacial resistance than those of the Celgard separator [22]. SiO_2 particles were introduced also in membranes based on polyimide (PI) nanofibers, leading to high conductivity ($2.27mScm^{-1}$) due to the excellent electrolyte wettability [23]. Finally, poly(phenylene oxide) (PPO)/mesoporous silica composite separators were prepared by a non-solvent induced phase separation (NIPS) process, the composite showing superior electrolyte wettability and thermal stability than the pristine polymer [24].

Therefore, considering that SiO_2 fillers improve the performance of separators and that PVDF is an excellent polymer matrix for Li-ion battery, the main goal of this work is to prepare PVDF/SS composites membranes by NIPS in order to improve electrolyte uptake, ionic conductivity and electrochemical properties. The silica spheres (SS) were synthetized by sol-gel method with the objective to obtain mesoporous structures with large BET (Brunauer-Emmett-Teller) surface area. The influence of the time exposure to air during sample processing by NIPS in the microstructure of the membrane was studied and correlated with the electrochemical performance of the battery separator. During the preparation of the membranes other processing parameters such as non-solvent (water), temperature of the non-solvent (25°C) and amount of SS (25wt%) were maintained constant. Those conditions were selected based on previous works in order to obtain PVDF with a high degree of porosity [25] and a maximum amount of SiO_2 within the polymer composite allowing to maintaining mechanical integrity, high electrolyte uptake and processability [21,26].

Experimental details

Materials

Poly(vinylidene fluoride) (PVDF, Solef 1010 and 5130), C-LiFePO $_4$ (LFP), carbon black (Super P-C45), N-methyl-2-pyrrolidone (NMP, Fluka) and N,N-dimethylformamide (DMF) were supplied by Solvay, Phostech Lithium, Timcal Graphite & Carbon and Merck, respectively. 1 M lithium hexafluorophosphate ($LiPF_6$) in ethylene carbonate- dimethyl carbonate (EC-DMC) 1: 1vol/vol solution was acquired by Solvionic

Sodium hydroxide (NaOH), concentrated ammonium solution (NH4OH) 28-30%, cetyltrimethylammonium bromide (CTABr), tetraethyl orthosilicate (TEOS) and absolute ethanol were purchased from Sigma-Aldrich. Ultrapure and deionized water were prepared in the laboratory.

Synthesis of mesoporous silica spheres

Mesoporous SS were synthesized by the sol-gel method adapting the method described in [27]. The main experimental steps for their production are shown in Fig. 1.

In short, 75 ml of NH_4OH were slowly added to 250 ml of deionized Milli-Q water and adjust the final volume to 1000 ml with deionized water. 4 g of CTABr were added at 35°C and left under magnetic stirring at 1000 rpm for 60 min .

16 ml of TEOS were then added drop-by-drop under mechanical stirring at 1500 rpm for 2 h at room temperature. Then, the solution was filtered and washed several times with ethanol and water and dried in an oven at 50°C for 1 h . Finally, the powder was calcined for 12 h at 550°C at a heating rate of $5°Cmin^{-1}$.

Composites membrane preparation

Membranes of PVDF with dispersed SS were prepared NIPS technique as illustrated in Fig. 2. More details on this method for obtaining porous membranes can be found in [28].

First, 0.5 g of SS were dispersed in 10 ml of DMF in an ultrasonic bath (Ultrasons Selecta ^{P}). 1.98 g of PVDF 1010 powder were added to the previous solution and dissolved under magnetic agitation during 3 h at 50°C. The PVDF/DMF volume fraction corresponds to 10% [28]. After cooling to room temperature, the solution was casted uniformly on clean and highly polished glass substrates (15 cm × 10 cm) by means of a hand-casting knife with a gap of 200μ m. The composite films were then immersed in a coagulation bath composed by water at 25°C after a preset time exposure of 1,5 or 20 min to air at 20°C and humidity of 65%. For the pristine film without SS, the time exposure to air was 20 min before immersed in the coagulation bath. The filler concentration within the polymer is 25wt%.

The prepared samples were identified as pristine and, for the composite membranes, by the time exposure to air, i.e, 1,5 and 20 min .

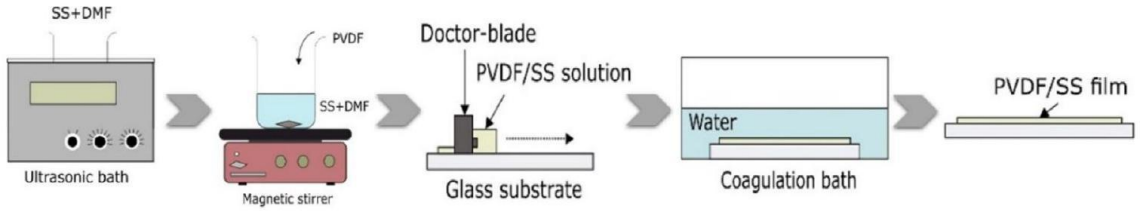

Fig. 2. Main experimental steps for the processing of PVDF/SS membranes by the NIPS method.

Characterization of the samples

Mesoporous SS

Transmission electron microscopy (TEM) measurements were performed with a Tecnai T20 from FEI. The TEM samples were dispersed in ethanol and dried onto a copper grid coated with carbon and analyzed at an operating voltage of 120 kV .

The surface area of the silica nanoparticles was determined by nitrogen adsorption-desorption experiments at $-196^{\circ}C$ with a TriStar 3000 analyzer, from Micromeritics, and using the Brunauer-Emmett-Teller (BET) equation. The X-ray diffraction (XRD) spectroscopy was carried out with a Bruker D8 Discover diffractometer using CuKa incident radiation.

PVDF/SS membranes

Membranes were coated with a thin gold layer using a sputter coater (Polaron, model SC502 sputter coater) and their morphology was analyzed using a scanning electron microscopy (SEM) (FEI Quanta 650 FEG microscope), equipped with an INCA 350 spectrometer from Oxford Instruments for energy dispersive X-ray spectroscopy (EDX).

The polymer phase of the membranes was determined by Fourier transformed infrared spectroscopy (FTIR) spectra using a FTIR 4100 system, Jasco in attenuated total reflection (ATR) mode over a range of $650 - 4000\ cm^{-1}$ with a resolution of $4\ cm^{-1}$. 64 scans were performed to each membrane.

The β-phase content of the membranes was calculated from the FTIR spectra by applying [29]:

$$F(\beta) = \frac{X_\beta}{X_\alpha + X_\beta} = \frac{A_\beta}{(K_\beta/K_\alpha)A_\alpha + A_\beta} \times 100 \quad (1)$$

where, $F(\beta)$ represents the β phase content; A_α and A_β the absorbencies at 766 and 840 cm^{-1}, corresponding to the α and β phase material, respectively; K_α and K_β are the absorption coefficient at the corresponding wave number and $X\alpha$ and $X\beta$ are the degree of crystallinity of each phase. The value of K_α and K_β are 6.1×10^4 and $7.7 \times 10^4\ cm^2\ mol^{-1}$, respectively.

The thermal properties of the membranes were determined by Differential scanning calorimetry (DSC) analysis. DSC was carried out in a Metter Toledo 821e apparatus under

a flowing nitrogen atmosphere between 25 and 200°C at a heating rate of $10°C min^{-1}$ for cooling and heating. All samples were measured in 40μ L aluminium pans with perforated lids to allow the release and removal of decomposition products.

The degree of crystallinity (χ_c) in % of the PVDF membranes was obtained by the following equation:

$$X_c = \frac{\Delta H_m}{x\left(\Delta H_{100\%\,\text{cryst.}}\right)_\alpha + y\left(\Delta H_{100\%\,\text{cryst.}}\right)_\beta} \times 100 \quad (2)$$

where x is the weight fraction of the α phase, y is the weight fraction of the β phase, $\left(\Delta H_{100\%\,\text{crystalline}}\right)_\alpha$ is the melting enthalpy of pure crystalline α-PVDF and ($\Delta H_{100\%\,\text{crystalline}}$) β is the melting enthalpy of pure crystalline β-PVDF which are reported to be 93.04 J/g and 103.4 J/g, respectively [29].
2.4.2.1. Degree of porosity and electrolyte uptake value. The degree of porosity of the membranes in % were measured by the pycnometer method and calculated using the following relation:
porosity $= \frac{W_2 - W_3 - W_s}{W_1 - W_3} \times 100$
where W_s is the mass of the sample, and W_1, W_2 and W_3 are the weight of the pycnometer filled with hexane, the weight after placing the sample in the pycnometer with additional hexane to complete the volume and the weight after removing the sample from the pycnometer, respectively.

The uptake value in % was obtained by immersing the membranes into the electrolyte solution (1M$LiPF_6$ in EC: DMC) through the following equation:
uptake $= \frac{m_i - m_0}{m_0} \times 100$
where m_0 is the weight of the dry membrane and m_i is the weight of the membrane after immersion in the electrolyte solution.
2.4.2.2. Ionic conductivity, tortuosity and MacMullin number. The ionic conductivity of the membranes were measured by impedance spectroscopy in an Autolab PGSTAT-12 (Eco Chemie) at frequencies between 500 mHz and 65 kHz at a temperature of 25°C and an amplitude of 10 mV using a constant volume support equipped with gold blocking electrodes placed within a Buchi TO 50 oven.

The ionic conductivity (σ_{eff}) was determined by:

$$\sigma_{eff} = \frac{d}{R_b \times A} \quad (5)$$

where R_b is the bulk resistance (Ω), d is the thickness (cm) and A is the area of the separator membrane (cm^2).

Tortuosity (τ) and MacMullin number (N_M) are relevant parameters for the separators and were determined by Eqs. (6) and (7), respectively:

$$\sigma_{\text{eff}} = \sigma_0 \frac{\varepsilon}{\tau^2} \quad (6)$$

$$N_M = \frac{\sigma_0}{\sigma_{eff}} \quad (7)$$

where σ_0 is the conductivity of the pure liquid electrolyte, σ_{eff} is the room temperature conductivity of the membrane plus the liquid electrolyte and ε is the degree of porosity of the membrane.

Electrode preparation, Li/C_LiFePO_4 cell manufacturing and testing

The electrode slurry was prepared by mixing of LFP, Super P, and the PVDF 5130 polymer binder in NMP solvent with a weight ratio of 80:10:10 (wt%), respectively. More details of electrode slurry preparation can be found in [30].

2016 coin-type for Li/LFP half-cells were assembled inside an argon-filled glovebox where 0_2 and H_20 level kept bellow 0.1 ppm . The metallic lithium foil (10 mm diameter) was used as counter and reference electrodes, the as prepared composite membranes soaked with $LiPF_6$ in Ethylene carbonate and diethylene carbonate (1:1) electrolyte solution were used as separator (14 mm diameter) and the prepared LFP

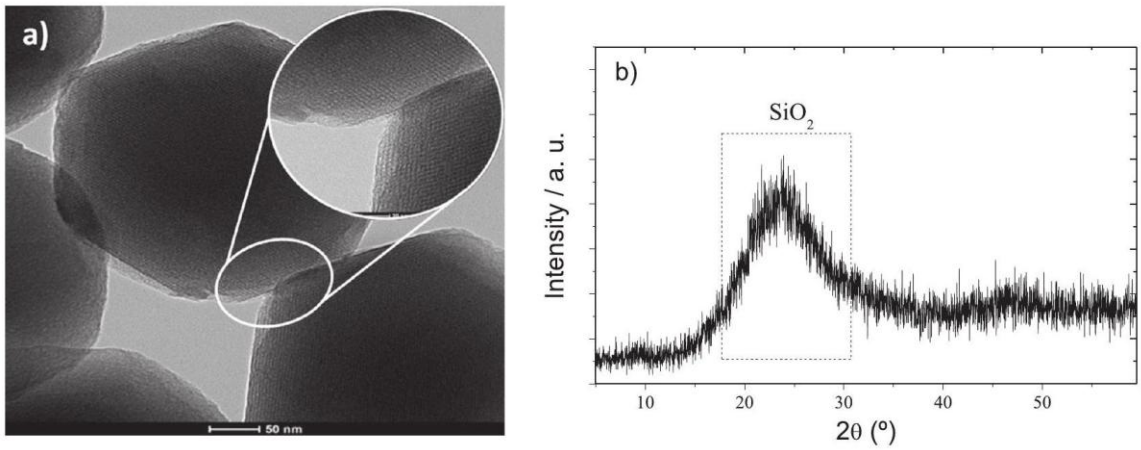

Fig. 3. Representative TEM image (a) and XRD pattern (b) of the synthesized mesoporous SS.

electrode film (10 mm diameter) served as cathode.
The cycling performance of the Li/LFP half-cells were evaluated at room temperature using a multichannel Maccor 4200 potentiostat. The galvanostatic measurements were performed in the potential window of $2.5 - 4.2$ V at various C - rates ranging from $C/10 - 2C$ ($C = 170 mAhg^{-1}$).

Electrochemical impedance spectroscopy (EIS) was measured with an Autolab PGSTAT12 instrument at a frequency range from 1 MHz to 10 mHz with an amplitude of 10 mV .

Results and discussion

Mesoporous SS

The size, morphology and crystalline structure of the mesoporous SS were evaluated by TEM and XRD, respectively. The results are shown in Fig. 3.

Fig. 3a) shows that the SS are characterized by an hexagonal shape (see also Supplementary information, Fig. S1), which is typical for this synthesis method [27]. The particles are characterized by a very homogeneous mesoporous arrangement [31] and an average diameter of 383 ± 56 nm The porous nature of the SS after calcination is also confirmed by the BET results that demonstrate a high surface area of approximately 1197 $m^2\ g^{-1}$.

The XRD pattern of the silica nanoparticles is shown in Fig. 3b). It can be observed a broadband centered at $2\theta = 23.6°$, corresponding to the amorphous phase of the silica [32].

Morphology, polymer phase and thermal properties of the PVDF/SS membranes

The morphology of the processed membranes, including pristine and PVDF/SS samples obtained by NIPS is presented in the SEM images of Fig. 4. Moreover, the EDS spectra of the pristine and the composite membranes after 1 min of exposure to air (representative also for the rest of the composites) are shown in the insert of Fig. 4a-b), respectively.

All membranes present a porous morphology with microvoids formed from the interconnected spherulitic structure typical of PVDF [33]. This morphology is dependent on the diffusion kinetics, i.e., solvent and non-solvent transfer rate [34] and is due to liquid-liquid demixing where the phase separation occurs due to the high affinity between solvent and nonsolvent [34]. No nanoparticle agglomerates are observed, indicating a suitable distribution of the SS nanoparticles all along the polymer membrane. The degree of porosity of the membranes, calculated by using Eq. (3) and is shown in Fig. 6a. It can be noticed that the size of the spherulites decreases and their number increases with the addition of the SS (Fig. 4b-d), when compared to the pristine membrane (Fig. 4a), showing that these fillers act as nucleating agents for polymer crystallization [35].

For the composite membrane immersed in water after a time exposure to air of 1 min (Fig. 4b), a heterogeneous morphology is observed with a larger spherulite roughness.

The composite membranes obtained after exposure to air for 5 min and 20 min (Fig. 4c and d) show a very similar porous morphology, the exposure time difference not affecting the sample morphology. The reason for this behavior is due to the fact that the crystallization time is sufficient to become irreversible and to overlap the liquid-liquid demixing process that occurs within the coagulation bath [34].

EDS spectrum show the characteristic peaks of C and F for the pristine membrane (insert of the Fig. 4a). In relation to the composite membrane, insert of the Fig. 4b) shows, together with the elements characteristic of PVDF, the characteristic peaks of O and Si elements, corresponding to the silica nanoparticles.

The infrared spectra of the processed membranes are shown in Fig. 5a and will allow to identify and quantify the crystalline phases of PVDF in each sample.

The characteristics bands of PVDF (α-phase at 766 cm^{-1} and β phase 840 cm^{-1}) and of the SS are identified in the Fig. 5a [29,36].

These results demonstrate that the addition of SS to PVDF matrix, as well as the exposure time to air, does not affect the α phase and β phases vibration peaks of the polymer.

Independently of the processing conditions, it is observed a high amount of the β phase above 90%, calculated using Eq. (1), which is justified by the low evaporation temperature and, therefore, low solvent evaporation kinetics and slow crystallization. It has been reported that lower polymer-chain mobility leads to crystallization of the polymer in the highly polar β-phase [37,38].

All membranes also show the vibration band at $1069\ \mathrm{cm}^{-1}$ corresponding to CF_2 (symmetric stretching) and CH_2 (w, wagging), typical of PVDF [39].

Moreover, the FTIR-ATR spectra of the composite membranes reveals the broad band centered at around $966\ \mathrm{cm}^{-1}$ and $1065 - 1095\ \mathrm{cm}^{-1}$ corresponding to the in-plane stretching vibration of $Si - O$ and antisymmetric stretching vibration of $Si - O - Si$, respectively, ascribed to the presence of the SS [36].

The thermal behavior of the membranes was determined by differential scanning calorimetry (DSC) and the thermographs are presented in Fig. 5b).

All membranes show a single melting peak between 165 and 170°C

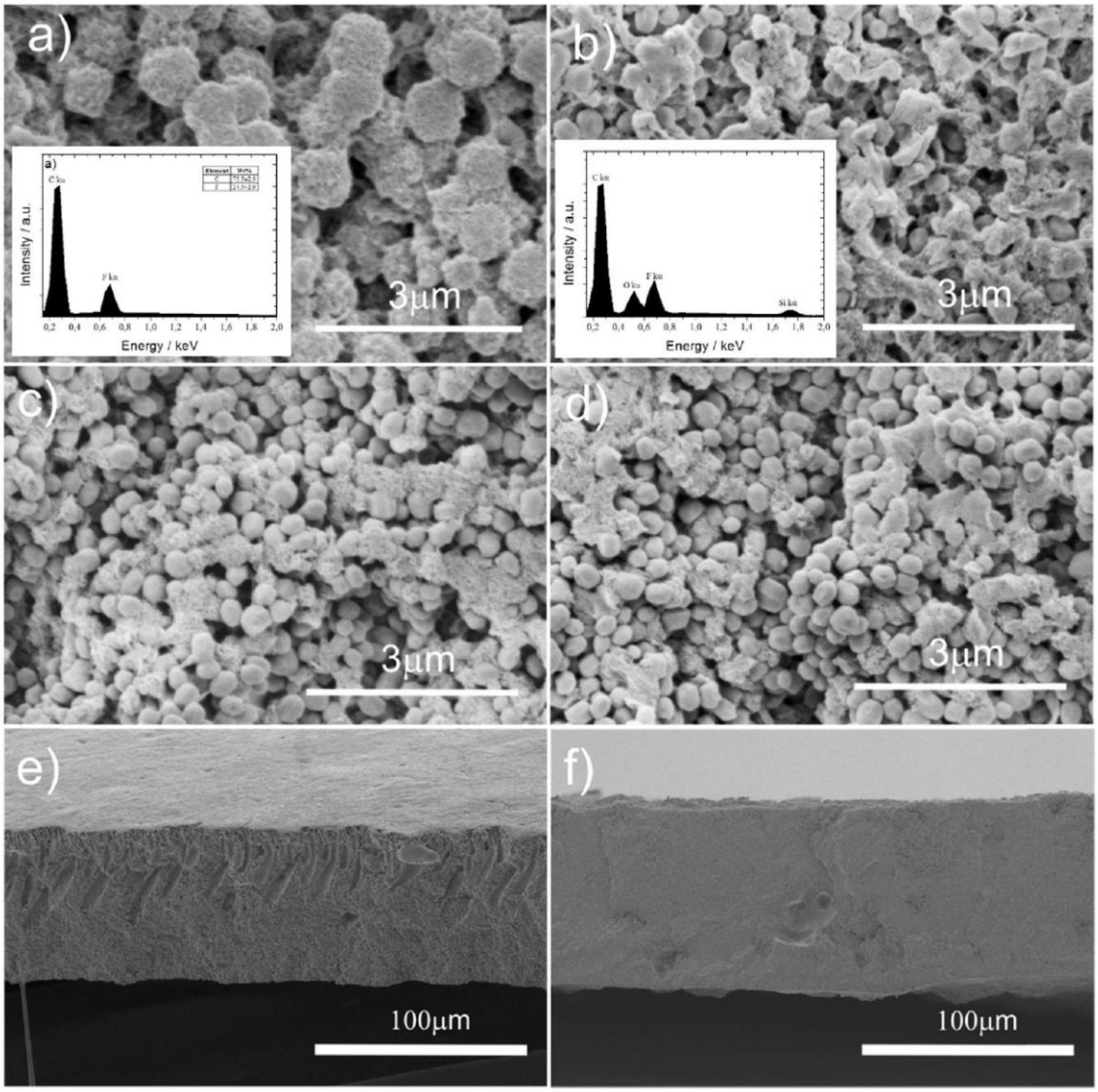

Fig. 4. Representative SEM images of the microstructure of the membranes prepared by NIPS for the (a) pristine PVDF membrane and the (b-d) composite PVDF/SS membranes obtained after an exposure time to air of 1,5 and 20 min before immersion in the water coagulation bath, respectively. Cross section images of the membrane prepared after 1 min exposure to air (e) and representative cross-section image for other all membranes prepared (f). The insets show the corresponding EDS spectra. except for the pristine membrane where is observe the existence of the double peak attributed to the increase of lamellae thickness, i.e. the interlamella diffusion of the polymer chains [40]. The degree of crystallinity calculated by Eq. (2) from the DSC and for all samples, is 54 ± 3%. These results show that the melting temperature and degree of crystallinity of the composites membranes is not is affected by the exposure time to air within experimental error but slightly decreases compared to the pristine membrane due to the addition of SS that can lead to defects in the crystalline structure.

The high degree of crystallinity obtained for all membranes is typical for PVDF and is dependent on the crystalline phase present in the PVDF membranes and the processing

conditions [40].

3.3. Porosity, uptake and electrochemical properties of the PVDF/SS membranes

In order to obtain an efficient absorption of the liquid electrolyte, the degree of porosity is an important property for battery separator. The degree of porosity for the different membranes ae presented in Fig. 6a.

Fig. 6a shows that the degree of porosity increases for the composite membranes in comparison with the pristine membrane, the SS affecting the phase separation process of the polymer and also the degree of porosity of the fillers.

On the other hand, the degree of porosity of the composite membranes is not significantly affected by the exposure time to air, being the variations within experimental error.

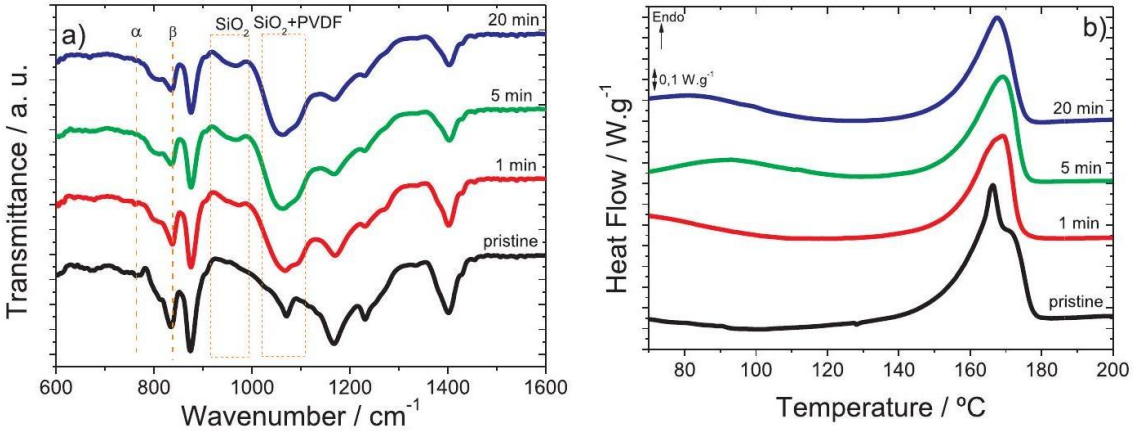

Fig. 5. (a) FTIR-ATR spectra and (b) DSC thermographs of the processed membranes.

Typically, the degree of porosity of commercial separators for Li-ion batteries ranges from 38% to 60%, depending on the type of separator [41].

The absorption of an electrolyte solution by a separator is a key parameter for the performance of lithium-ion batteries and it is related to the surface chemistry and the degree of porosity [42].

Fig. 6b shows the uptake of the electrolyte solution for the all membranes as a function of the dipping time. In turn, independently of the membranes, Fig. 6b shows that the process is very fast and more than 80% of the uptake takes place in 30 s , which is attributed to the strong interactions between the organic electrolyte and the polar functional groups of PVDF, in particular when crystallized in the electroactive and polar β-phase [43,44]. The result also show that all membranes reach saturation after approximately 10 min indicating that the void volume has been filled in two stages: first, the electrolyte fill the pores and then it is absorbed into the amorphous phase of PVDF [45].

It is to notice that the membrane with the highest uptake value is the composite membrane prepared after 1 min exposure to air, which is be related to the presence of finger-like pores in the cross-section of this membrane (Fig. 4e) and also because of the more homogeneous distribution of the SS through the membrane that show to be less compact than the other (Fig. 4f).

Thus, comparing the pristine membrane and the composite membrane with 1 min exposure to air, it seems that the presence of SS combined with a precise exposure time to air before immersion in the water coagulation bath result in a positive effect on the uptake of the liquid electrolyte, i.e, increasing its uptake value. However, an increase of the time exposure to air has a negative effect on the uptake value as it decreases and shows values lower than the pristine membrane. This result is related to morphological variations of the membranes, as previously stated, that demonstrate a more compact porous morphology, even with similar porosity values, for higher exposure time to air (Fig. 4).

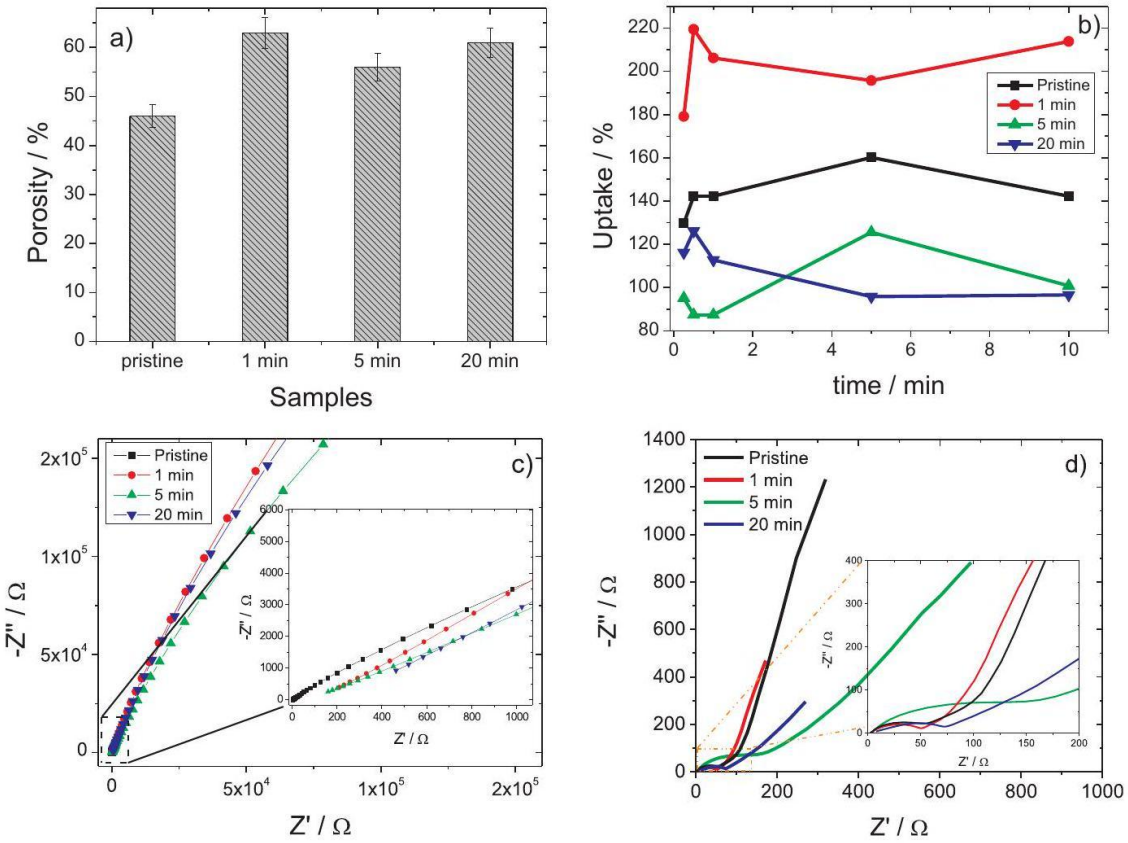

Fig. 6. (a) Degree of porosity, (b) uptake value, (c) Nyquist plots of gold/separator/gold and (d) impedance plots of Li/separator/LFP cells before cycling of the processed membranes.

Table 1
Ionic conductivity, tortuosity (τ), MacMullin number (N_M) and total resistance (R_{total}) for the processed membranes.

Samples	σ_{eff} /mScm^{-1}	T	N_M	R_{total} /Ω
Pristine	1	2	12	58
1 min	0.9	3	15	50
5 min	0.4	4	29	151

20 min	0.1	8	118	73

The Nyquist plot at 25°C of the processed membranes embedded in the liquid electrolyte is shown in Fig. 6c and is characterized by an inclined straight line in all frequency range.

This behavior is related to the diffusion process of the polymer chains, resulting a low impedance as illustrated in Fig. 6c [45].

The ionic conductivity values were calculated by Eq. (5) and are presented in Table 1. The resistance values are determined from the high-frequency side by the intersection of the straight line with the real axis. It is observed that the ionic conductivity is practically the same for the pristine and the composite membrane prepared after 1 min exposure to air but this value decreases when the air exposure time increases, which is correlated to the uptake value.

In addition to the ionic conductivity, Table 1 shows the tortuosity and the MacMullin number (N_M) calculated using Eqs. (6) and (7), respectively. The tortuosity value of the membranes varies between 2 and 8 where the ideal value is 1 . This result indicates that the conductivity path is not completely uniform parallel to the transport direction. A lower tortuosity value is observed for the pristine membrane and composite membrane prepared after an exposure time to air of 1 min , which supports better pore connectivity [45].

In relation to the MacMullin number (N_M), the obtained values are between 12 and 118, correlating with the uptake value between the membrane and the electrolyte solution [43]. It is also observed, that the lower value of the MacMullin number was obtained for the pristine membrane and its value increases with the increase of exposure time to air.

Fig. 6d shows the ac impedance spectra of the cathodic half-cells obtained before cycling in open circuit voltage (OCV) for the different membranes.

Fig. 6d shows a semicircle in the high and medium frequency range that represents the overall resistance that is the sum of the ohmic resistance, resistance that represents the contact film resistance (solid electrolyte interface (SEI)) and the resistance contributions from the charge-transfer reaction, as well as straight line in the low frequency region that represents the diffusion of lithium ions in the active material of the cathode electrode [30].

Table 1 shows the overall resistance calculated from Fig. 6d for all processed membranes. It is observed that the composite membrane prepared after 1 min exposure to air present lower resistance value (50Ω) in comparison to the other membranes, indicating better interface stability that is the base for obtaining improved battery performance. Also, the addition of SS leads to a decrease of the resistance value for lower exposure time to air in comparison to pristine membrane, the exposure time to air affecting the resistance value through morphological variations of the membrane.

Battery performance of the PVDF/SS membranes in Li/LFP half-cells

Charge-discharge behavior of Li/LFP coin cells with the different processed membranes as separators were assembled and evaluated at room temperature as shown in Fig. 7.

Fig. 7a shows the charge-discharge profile in the fifth cycle at different C-rates from C/10-2 C for the composite membrane prepared after 1 min exposure to air.

Fig. 7a shows the typical flat voltage plateau at around 3.4 V indicating the presence of a two-phase Fe^{2+}/Fe^{3+} redox reaction between $FePO_4$ and $LiFePO_4$, the plateau being independent of the scan rate and cycle number [46].

The flat voltage plateau is detected up to C-rate, but for 2 C-rate an oblique line is distinguished that represents a capacitive storing behavior (Fig. 7a) [47].

Fig. 7a also shows that the charge-discharge profiles decrease with increasing C rate due to the influence of ionic transport on ohmic polarization but also on the interfacial reaction resistance on the lithium electrode [48]. The charge-discharge behavior represented in Fig. 7a is also representative for the other membranes (data not shown).

For the composite membranes prepared after 1 min exposure to air, the discharge capacity value is $149 mAhg^{-1}, 146 mAhg^{-1}$, $139 mAhg^{-1}, 127 mAhg^{-1}$ and $118 mAhg^{-1}$ at rates of C/10, C/5, C/2, C and 2C, respectively, which corresponds to $88\%, 86\%, 82\%$, 75% and 70% of the theoretical capacity of $C - LiFePO_4 (170\ mA\ h\ g^{-1})$, indicating a good electrochemical stability even at higher C rates. The high discharge capacity values of these membranes are related to their ionic conductivity and indicate improved rate capability and excellent affinity towards the electrolyte through of its porous structure.

Fig. 7b represents the fifth charge-discharge curve at 2 C for the different membranes. At 2 C , the voltage profile is stable with an oblique line, and the discharge capacities are $118 mAhg^{-1}, 111 mAh\ g^{-1}, 83 mAhg^{-1}$, and $75 mAhg^{-1}$ for the composite membrane prepared after 1 min exposure to air, the pristine membrane, and the composite membrane with 20 min and 5 min exposure to air, respectively. This charge-discharge behavior for all membranes is correlated with their ionic conductivity value and also with the uptake process, where the addition of SS stabilizes the electrode interfacial resistance and facilitates the migration of lithium ions at this interface [49].

Fig. 7c shows the rate performance of 5 cycles for each rate from $C/10 - 2C$ in the charge process of the membranes.

It is observed that the cycling performance is quite stable for the pristine membrane and the composite membrane for 1 min exposure to air. Whereas, the capacity decreases more rapidly for the composite membranes prepared after 5 and 20 min exposure to air, independently of the C rate.

Until C/2-rate, the capacity values are very similar for all membranes. For rate above 1 C , the capacity value decreases in the following order: composite membrane 1 min > pristine membrane > composite membrane 20 min > composite membrane 5 min , which is in agreement with the uptake values correlated with the variation of the microstructure.

Fig. 7d shows the charge capacity retention as a function of C-rate calculated through the normalization of the delivered capacity for each C-rate with respect to the nominal value for C/10 rate. For all membranes, it is observed that the capacity retention decreases with increasing C-rate, which is associated to the diffusion phenomena taking place within the electrode active material phase and the separator membrane soaked with the electrolyte solution [50]. The capacity fading is more pronounced for the composite membranes with

20 min and 5 min exposure to air due to low efficiency lithium ions transport between the electrodes.

For composite membrane for 1 min exposure to air, at 2C (charge and/or discharge process in half an hour), the capacity retention is 79% which is superior when compared with other PVDF based separator membranes, such as PVDF-HFP [50] and PVDF-TrFE/PEO [45] membranes.

Taking into account the good rate capability of all membranes (Fig. 7c), Fig. 8 shows their cycle stability at C/5 and 2C-rate for 50 cycles.

For C/5-rate (Fig. 8a), it is observed an excellent capacity value and good stability for all membranes.

In relation to 2C-rate (Fig. 8b), the cycling behavior with best performance is for the composite membrane for 1 min exposure to air, being practically constant as a function of the number of cycles with a

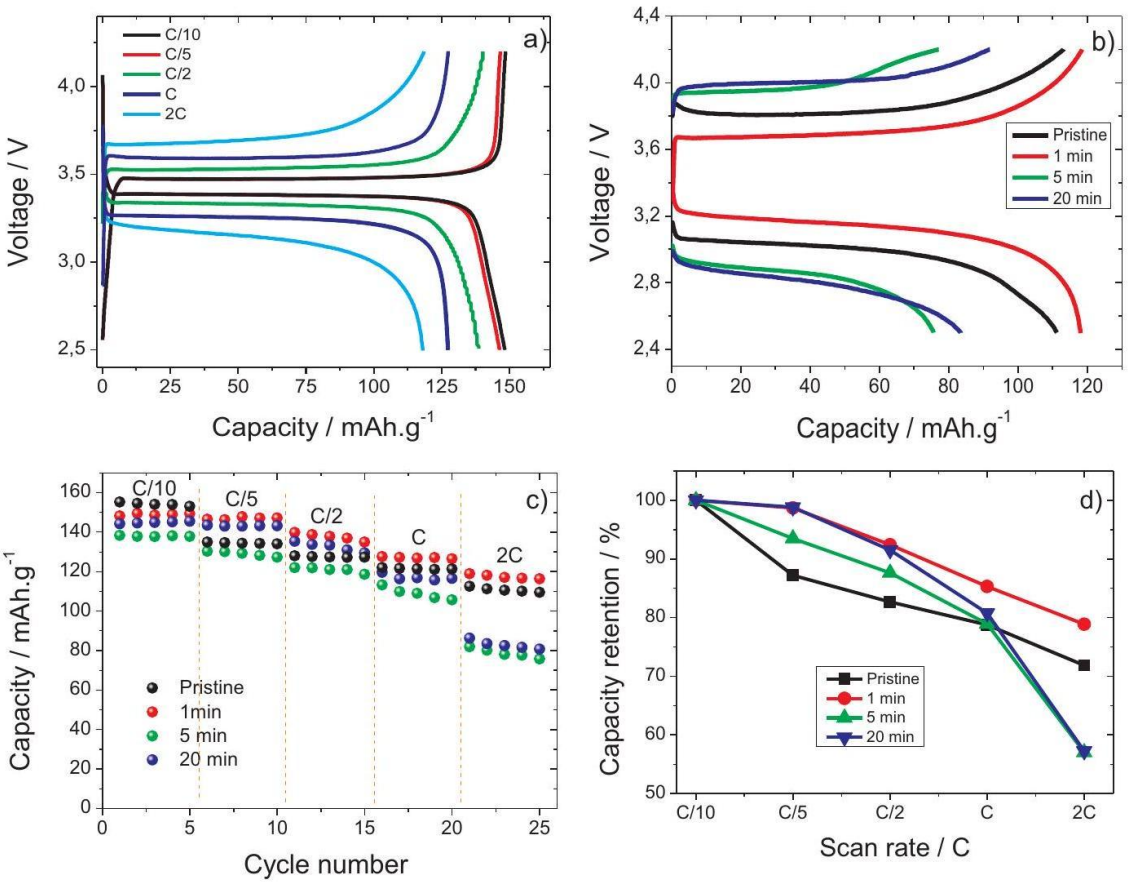

Fig. 7. Charge-discharge profiles for the composite membrane prepared after 1 min exposure to air (a). For the different processed membranes: 2 C rate (b), rate performance as a function of cycle number (c), and capacity retention (d) during the discharge process.

capacity fade of 4%.

Further, the coulombic efficiency presented in Fig. 8b) and related to the reversibility of the process is ~ 100% for all membranes independently of the number of cycles.

Considering the excellent charge-discharge results presented in Figs. 7 and 8, Table 2 compares the electrochemical properties of the composite membranes with best performance in this work with other membranes with silica reported in the literature for the same electrode and $LiMn_2O_4$.

Table 2 shows that the electrochemical results of the present work are similar or even better for high C-rates to the ones reported in the literature for other separators membranes with silica fillers.

Taking into account that the membrane with the best cycling performance is the composite membrane prepared after 1 min exposure to air and comparing the results at room temperature with Whatman glass microfiber separators [53] ($127 mAhg^{-1}$ for C rate for discharge capacity value) reported in the literature for the same active material but with smaller mass, it can be concluded that the battery performance reported in the present work is excellent and the developed separators represent a suitable alternative to commercial separators.

Considering that the used method allows to obtain membranes in a controlled and reproducible way and the addition of mesoporous SS into PVDF matrix improves battery performance in comparison to the pristine membranes in terms of reduced capacity fade, the novel composite membrane proposed in this work represents a promising separator for lithium-ion battery applications.

Conclusions

Silica/poly(vinylidene fluoride) composites prepared by non-

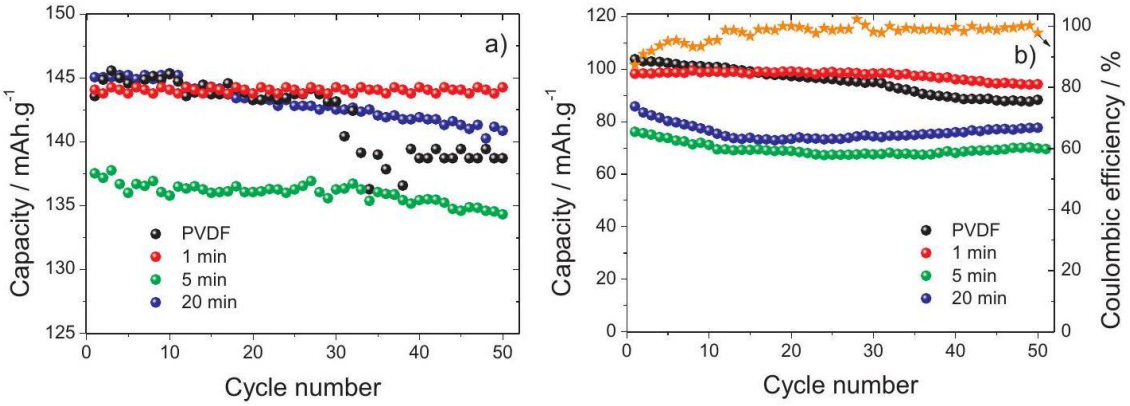

Fig. 8. Cycling performance of the membranes when cycled at C/5 (a) and 2C (b).

Table 2
Electrochemical parameters for different composites membranes with silica as fillers.

Polymer	Silica Size/nm	Electrolyte uptake/%	Ionic conductivity/mS cm	Capacity/mA hg $^{-1}$	Ref
PVDF	7	-	-	120@ C	[20]
PVDF-HFP coated	300	-	2.57	140@ C/5	[51]
PVDF/PAN	12	~ 430	1.68	150@ C at 60 °C	[21]
PVDF/PMMA nonwoven	25	406	4	158@ C/2	[22]
PI	15	2400	2.27	102@ C ($LiMn_2O_4$)	[23]
PS-co-PBA coated	70	-	0.7	145@ C/5	[52]
PPO	300	357	2.62	142@ C/2	[24]
PVDF	383	214	0.9	118@2C	This work

solvent induced phase separation (NIPS) have been investigated for li-thium-ion battery separator applications. The composites membranes were prepared with different air exposure time before immersion in the water coagulation bath for the same amount of silica spheres (SS). Mesoporous SS were synthetized by sol-gel method with an average size of ~ 400 nm. The morphology, degree of porosity, uptake value and electrical properties of the composites are influenced by the time of exposure to air and the presence of *SS*.

It is demonstrated that the characteristics of the membranes and their thermal properties are not influenced by the time of exposure to air and the presence of silica. Further, the composite membrane prepared with 1 min exposure to air, showed the best ionic conductivity of $0.9 mScm^{-1}$.

The electrochemical performance of $Li/C-LiFePO_4$ half-cells prepared with the composite membrane for 1 min exposure to air as separator, showing a discharge capacity value between $149 mAhg^{-1}$ at C/10 and $118 mAhg^{-1}$ at 2 C , respectively. Further at 2 C it is observed a high capacity retention of 79% and after 50 cycles at 2 C -rate, the capacity fade of this separator is 4%, which is lower when compared with the pristine membrane (16%).

Thus, the excellent electrochemical performance including capacity retention, rate capability and cyclability of this composite membrane, indicates its suitability as perspective separator for lithium-ion batteries.

Acknowledgments

The authors thank the FCT (Fundação para a Ciência e Tecnologia) for financial support under the framework of Strategic Funding grants UID/FIS/04650/2013, UID/EEA/04436/2013 and UID/QUI/0686/ 2016; and project no. POCI-01-0145-FEDER-028157. The authors also thank the FCT for financial support under grants SFRH/BPD/112547/ 2015 (C.M.C.) and SFRH/BPD/98109/2013 (V.F.C.) and Nanochem group of INL. Financial support from the Spanish Ministry of Economy and Competitiveness (MINECO) through project MAT2016-76039-C4-3-R (AEI/FEDER, UE) (including FEDER financial support) and from the Basque Government Industry Department under the ELKARTEK and HAZITEK Program is also acknowledged.

References

[1] R.A. Kerr, R.F. Service, What can replace cheap oil-and when? Science 309 (2005) (101-101).
[2] J.P. Holdren, Energy and sustainability, Science 315 (2007) (737-737).
[3] J.M. Tarascon, M. Armand, Issues and challenges facing rechargeable lithium batteries, Nature 414 (2001) 359.
[4] C.A. Vincent, Lithium batteries: a 50-year perspective, 1959-2009, Solid State Ion. 134 (2000) 159-167.
[5] C.M. Costa, M.M. Silva, S. Lanceros-Mendez, Battery separators based on vinylidene fluoride (VDF) polymers and copolymers for lithium ion battery applications, RSC

Adv. 3 (2013) 11404-11417.
[6] Y.S. Chung, S.H. Yoo, C.K. Kim, Enhancement of meltdown temperature of the polyethylene lithium-ion battery separator via surface coating with polymers having high thermal resistance, Ind. Eng. Chem. Res. 48 (2009) 4346-4351.
[7] G. Venugopal, J. Moore, J. Howard, S. Pendalwar, Characterization of microporous separators for lithium-ion batteries, J. Power Sources 77 (1999) 34-41.
[8] B.K. Choi, K.H. Shin, Y.W. Kim, Lithium ion conduction in PEO-salt electrolytes gelled with PAN, Solid State Ion. 113-115 (1998) 123-127.
[9] Y. Kang, H.J. Kim, E. Kim, B. Oh, J.H. Cho, Photocured PEO-based solid polymer electrolyte and its application to lithium-polymer batteries, J. Power Sources 92 (2001) 255-259.
[10] B. Huang, Z. Wang, G. Li, H. Huang, R. Xue, L. Chen, F. Wang, Lithium ion conduction in polymer electrolytes based on PAN, Solid State Ion. 85 (1996) 79-84.
[11] D. Djian, F. Alloin, S. Martinet, H. Lignier, Macroporous poly(vinylidene fluoride) membrane as a separator for lithium-ion batteries with high charge rate capacity, J. Power Sources 187 (2009) 575-580.
[12] C.M. Costa, L.C. Rodrigues, V. Sencadas, M.M. Silva, G. Rocha, S. Lanceros-Méndez, Effect of degree of porosity on the properties of poly(vinylidene fluoride-trifluorethylene) for Li-ion battery separators, J. Membr. Sci. 407-408 (2012) 8.
[13] C.M. Costa, L.C. Rodrigues, V. Sencadas, M.M. Silva, S. Lanceros-Méndez, Effect of the microsctructure and lithium-ion content in poly[(vinylidene fluoride)-co-trifluoroethylene]/lithium perchlorate trihydrate composite membranes for battery applications, Solid State Ion. 217 (2012) 19-26.
[14] J. Nunes-Pereira, C.M. Costa, S. Lanceros-Méndez, Polymer composites and blends for battery separators: state of the art, challenges and future trends, J. Power Sources 281 (2015) 378-398.

[15] V. Di Noto, S. Lavina, G.A. Giffin, E. Negro, B. Scrosati, Polymer electrolytes: present, past and future, Electrochim. Acta 57 (2011) 4-13.
[16] F. Croce, L. Persi, B. Scrosati, F. Serraino-Fiory, E. Plichta, M.A. Hendrickson, Role of the ceramic fillers in enhancing the transport properties of composite polymer electrolytes, Electrochim. Acta 46 (2001) 2457-2461.
[17] H. Liu, Z. Dai, J. Xu, B. Guo, X. He, Effect of silica nanoparticles/poly(vinylidene fluoride-hexafluoropropylene) coated layers on the performance of polypropylene separator for lithium-ion batteries, J. Energy Chem. 23 (2014) 582-586.
[18] M. Yanilmaz, C. Chen, X. Zhang, Fabrication and characterization of SiO2/PVDF composite nanofiber-coated PP nonwoven separators for lithium-ion batteries, J. Polym. Sci. Part B: Polym. Phys. 51 (2013) 1719-1726.
[19] P. Sivaprakash, S. Sivaprakash, SiO2/PVDF coated separator with enhanced thermal stability for Lithium-ion rechargeable batteries.
[20] M. Zaccaria, D. Fabiani, G. Cannucciari, C. Gualandi, M.L. Focarete, C. Arbizzani, F. De Giorgio, M. Mastragostino, Effect of silica and tin oxide nanoparticles on properties of nanofibrous electrospun separators, J. Electrochem. Soc. 162 (2015) A915-A920.
[21] W. Zheng, Y. Zhu, B. Na, R. Lv, H. Liu, W. Li, H. Zhou, Hybrid silica membranes with a polymer nanofiber skeleton and their application as lithium-ion battery separators, Compos. Sci. Technol. 144 (2017) 178-184.
[22] Q. Fu, G. Lin, X. Chen, Z. Yu, R. Yang, M. Li, X. Zeng, J. Chen, Mechanically reinforced PVdF/PMMA/SiO2 composite membrane and its electrochemical properties as a separator in lithium-ion batteries, Energy Technol. 6 (2018) 144-152.
[23] Y. Wang, S. Wang, J. Fang, L.-X. Ding, H. Wang, A nano-silica modified polyimide nanofiber separator with enhanced thermal and wetting properties for high safety lithium-ion batteries, J. Membr. Sci. 537 (2017) 248-254.
[24] Y. Lv, B. Gu, Mesoporous silica particles-embedded high performance separator for lithium-ion batteries, J. Mater. Sci.: Mater. Electron. 28 (2017) 6512-6519.
[25] C.G. Ferreira, V.F. Cardoso, A.C. Lopes, G. Botelho, S. Lanceros-Méndez, Tailoring microstructure and physical properties of poly(vinylidene fluoride-hexafluoropropylene) porous films, J. Mater. Sci. 50 (2015) 5047-5058.
[26] K. Prasanna, C.-S. Kim, C.W. Lee, Effect of SiO2 coating on polyethylene separator with different stretching ratios for application in lithium ion batteries, Mater. Chem. Phys. 146 (2014) 545-550.
[27] V.F. Cardoso, S. Irusta, N. Navascues, S. Lanceros-Mendez, Comparative study of sol-gel methods for the facile synthesis of tailored magnetic silica spheres, Mater. Res. Express 3 (2016) 075402.
[28] C. Ribeiro, C.M. Costa, D.M. Correia, J. Nunes-Pereira, J. Oliveira, P. Martins, R. Gonçalves, V.F. Cardoso, S. Lanceros-Méndez, Electroactive poly(vinylidene fluoride)-based structures for advanced applications, Nat. Protoc. 13 (2018) 681.
[29] P. Martins, A.C. Lopes, S. Lanceros-Mendez, Electroactive phases of poly(vinylidene fluoride): determination, processing and applications, Progress. Polym. Sci. 39 (2014) 683-706.
[30] A. Gören, J. Mendes, H.M. Rodrigues, R.E. Sousa, J. Oliveira, L. Hilliou, C.M. Costa, M.M. Silva, S. Lanceros-Méndez, High performance screen-printed electrodes prepared by a green solvent approach for lithium-ion batteries, J. Power Sources 334 (2016) 65-77.
[31] M.A. Agotegaray, V.L. Lassalle, Silica-coated Magnetic Nanoparticles: An Insight into Targeted Drug Delivery and Toxicology, Springer International Publishing, Switzerland, 2017.
[32] C. Corcione, R. Striani, M. Frigione, Microgel modified UV-cured methacrylic-silica hybrid: synthesis and characterization, Materials 6 (2013) 3805.
[33] R. Magalhães, N. Durães, M. Silva, J. Silva, V. Sencadas, G. Botelho, J.L. Gómez

Ribelles, S. Lanceros-Méndez, The role of solvent evaporation in the microstructure of electroactive β-poly(vinylidene fluoride) membranes obtained by isothermal crystallization, Soft Mater. 9 (2010) 1-14.
[34] V.F. Cardoso, G. Botelho, S. Lanceros-Méndez, Nonsolvent induced phase separation preparation of poly(vinylidene fluoride-co-chlorotrifluoroethylene) membranes with tailored morphology, piezoelectric phase content and mechanical properties, Mater. Des. 88 (2015) 390-397.
[35] Y.Y. Zhang, S.L. Jiang, Y. Yu, G. Xiong, Q.F. Zhang, G.Z. Guang, Phase transformation mechanisms and piezoelectric properties of poly(vinylidene fluoride)/ montmorillonite composite, J. Appl. Polym. Sci. 123 (2012) 2595-2600.
[36] R. Al-Oweini, H. El-Rassy, Synthesis and characterization by FTIR spectroscopy of silica aerogels prepared using several Si(OR)4 and R′′Si(OR′)3 precursors, J. Mol. Struct. 919 (2009) 140-145.
[37] D.L. Chinaglia, R. Gregorio, J.C. Stefanello, R.A.P. Altafim, W. Wirges, F. Wang, R. Gerhard, Influence of the solvent evaporation rate on the crystalline phases of solution-cast poly(vinylidene fluoride) films, J. Appl. Polym. Sci. 116 (2010) 785-791.
[38] R. Gregorio, D.S. Borges, Effect of crystallization rate on the formation of the polymorphs of solution cast poly(vinylidene fluoride), Polymer 49 (2008) 4009-4016.
[39] V. Aravindan, P. Vickraman, Nanoparticulate Al0(OH) n filled polyvinylidene-fluoride-co-hexafluoropropylene based microporous membranes for lithium ion batteries, J. Renew. Sustain. Energy 1 (2009) 023108.
[40] C. Marega, A. Marigo, Influence of annealing and chain defects on the melting behaviour of poly(vinylidene fluoride), Eur. Polym. J. 39 (2003) 1713-1720.
[41] C.J. Weber, S. Geiger, S. Falusi, M. Roth, Material review of Li Ion battery separators, AIP Conf. Proc. 1597 (2014) 66-81.
[42] E. Quartarone, P. Mustarelli, A. Magistris, Transport properties of porous PVDF membranes, J. Phys. Chem. B 106 (2002) 10828-10833.
[43] C.M. Costa, H.M. Rodrigues, A. Gören, A.V. Machado, M.M. Silva, S. Lanceros-Méndez, Preparation of poly(vinylidene fluoride) lithium-ion battery separators and their compatibilization with ionic liquid - a green solvent approach, ChemistrySelect 2 (2017) 5394-5402.
[44] M. Kundu, C.M. Costa, J. Dias, A. Maceiras, J.L. Vilas, S. Lanceros-Méndez, On the relevance of the polar β-phase of poly(vinylidene fluoride) for high performance lithium-ion battery separators, J. Phys. Chem. C 121 (2017) 26216-26225.
[45] A. Gören, C.M. Costa, M.N. Tamaño Machiavello, D. Cíntora-Juárez, J. NunesPereira, J.L. Tirado, M.M. Silva, J.L. Gomez Ribelles, S. Lanceros-Méndez, Effect of the degree of porosity on the performance of poly(vinylidene fluoride-trifluoroethylene)/poly(ethylene oxide) blend membranes for lithium-ion battery separators, Solid State Ion. 280 (2015) 1-9.
[46] Y.-H. Nien, J.R. Carey, J.-S. Chen, Physical and electrochemical properties of LiFePO4/C composite cathode prepared from various polymer-containing precursors, J. Power Sources 193 (2009) 822-827.
[47] S.-X. Zhao, H. Ding, Y.-C. Wang, B.-H. Li, C.-W. Nan, Improving rate performance of LiFePO4 cathode materials by hybrid coating of nano-Li3PO4 and carbon, J. Alloy. Compd. 566 (2013) 206-211.
[48] W. Xiao, L. Zhao, Y. Gong, S. Wang, J. Liu, C. Yan, Preparation of high performance lithium-ion batteries with a separator-cathode assembly, RSC Adv. 5 (2015) 34184-34190.
[49] J. Cho, Y.-C. Jung, Y.S. Lee, D.-W. Kim, High performance separator coated with amino-functionalized SiO 2 particles for safety enhanced lithium-ion batteries, J . Membr. Sci. 535 (2017) 151-157.
[50] R.E. Sousa, J. Nunes-Pereira, C.M. Costa, M.M. Silva, S. Lanceros-Méndez, J.

Hassoun, B. Scrosati, G.B. Appetecchi, Influence of the porosity degree of poly (vinylidene fluoride-co-hexafluoropropylene) separators in the performance of Li ion batteries, J. Power Sources 263 (2014) 29-36.
[51] W. Xiao, J. Wang, H. Wang, Y. Gong, L. Zhao, J. Liu, C. Yan, Hollow mesoporous silica sphere-embedded composite separator for high-performance lithium-ion battery, J. Solid State Electrochem. 20 (2016) 2847-2855.
[52] H. Liao, H. Zhang, G. Qin, H. Hong, Z. Li, Y. Lin, L. Li, Novel core-shell PS-co-PBA@ SiO2 nanoparticles coated on PP separator as "thermal shutdown switch" for high safety lithium-ion batteries, Macromol. Mater. Eng. 302 (2017) 1700241.
[53] A. Gören, C.M. Costa, M.M. Silva, S. Lanceros-Mendez, Influence of fluoropolymer binders on the electrochemical performance of C-LiFePO4 based cathodes, Solid State Ion. 295 (2016) 57-64.